ORIGINAL RESEARCH

Territorial and Microvascular Perfusion Impairment in Brain Arteriovenous Malformations

J. Fiehler
T. Illies
M. Piening
D. Säring
N. Forkert
J. Regelsberger
U. Grzyska
H. Handels
J.V. Byrne

BACKGROUND AND PURPOSE: Both the existence and clinical relevance of a steal phenomenon in brain arteriovenous malformations (AVMs) remains a matter of debate. This study aimed to assess perfusion in the brain adjacent to brain AVMs and to relate these to macrovascular blood flow in a single measurement.

MATERIALS AND METHODS: Twenty consecutive patients with AVMs with a median age of 37 years were evaluated by 3T MR imaging by using 3D time-resolved MR angiography to determine blood flow and perfusion patterns. Cerebral perfusion was estimated by using an arterial spin-labeling technique in vascular territories around the nidus and in symmetric regions of interest in the ipsilateral and contralateral hemispheres. Mapping of concentric shells around the nidus was used to define the immediate and adjacent brain and relative perfusion reductions >20% of baseline, termed perinidal dip (PND).

RESULTS: A significant reduction in perfusion ratios between ipsilateral and contralateral hemispheres remote to the AVMs was demonstrated in the middle and posterior cerebral artery territories. PND was detected in 5 patients, and 17 patients overall showed reduced perfusion in the perinidal region on visual inspection. There was a negative correlation of the hemispheric territorial perfusion with the affected/nonaffected inflow time ratio ($R = -0.402$, $P = .015$).

CONCLUSIONS: The perfusion impairment in vascular territories adjacent to brain AVMs that we identified as PND may reflect the existence of 2 levels of perfusion impairment: a territorial and a microvascular perfusion disturbance. Although the hemispheric asymmetry in territorial perfusion seems the result of arterioarterial redistribution, the PND was inhomogeneously distributed within a single vascular territory and thus might result from low perfusion pressure in small arteries and arterioles.

The essential anatomic feature of brain arteriovenous malformations (AVMs) is the connection of arteries to abnormally tortuous and dilated veins that communicate directly within a nidus without interposing capillaries.[1] The missing capillary bed results in a low-resistance condition and causes high flow through the AVM with early venous filling. In the vicinity of the AVM nidus, where AVM feeders and neighboring normal vessels share the same proximal arterial origin, a "hypotensive zone" has been suggested, where capillary perfusion pressure is relatively low. In 1949, Norlén[2] reported disturbed contrast opacification of the normal intracranial circulation in patients with AVM, which improved after surgical resections of the AVM. This observation has been considered the first evidence of a steal phenomenon associated with AVMs.[3] Generally, the term "intracerebral steal" describes a pathologic process in which increased blood flow through a low-resistance vascular bed diverts flow away from adjacent brain. It has been defined as "reduction of blood flow within an area of already imperfectly perfused brain, under the influence of vasodilatation in neighboring zones."[4] The steal phenomenon has since been considered as a possible cause of neurologic symptoms, such as seizures and transient neurologic deficits, in patients with AVM.[3] However, this suggestion has been challenged,[5] and both its existence and clinical relevance in brain AVMs remain a matter of debate.

Perinidal capillary perfusion has been estimated by researchers by using a variety of techniques, including positron-emission tomography (PET),[6-10] single-photon emission CT (SPECT),[10-12] and MR imaging.[13,14] The problems encountered by using PET and SPECT to evaluate perinidal brain are due to their comparatively low spatial resolution, which requires that structures in the direct vicinity of the nidus be subject to the effects of partial voluming.[7,15] Previous dynamic susceptibility contrast-enhanced brain perfusion MR imaging studies in patients with brain AVMs overcame some of these drawbacks but revealed conflicting results: One study found no abnormalities in most patients,[14] whereas another group was able to discriminate 3 different types of perinidal perfusion disturbances.[13] However, the ability of this technique to assess perinidal perfusion is limited in the vicinity of large vessels and the nidus due to artifacts caused by contrast media within vascular structures and the changes it induces in the local magnetic field.

Using arterial spin-labeling MR imaging spatially coregistered to MR angiography (MRA) data with high spatial and temporal resolution, we aimed to overcome the problem of poor resolution to investigate perfusion in the vicinity of AVM structures and the pathophysiology of steal effects. The intention was to analyze patterns of perfusion impairment and to relate them to determine simultaneously arterial inflow rates: 1) in the large artery vascular territories, and 2) in the vicinity of the AVM nidus. We hypothesized that perinidal perfusion is usually decreased and that these changes are related to increases in blood flow velocity in the feeding arteries and veins.

Received May 17, 2008; accepted after revision September 9.

From the Departments of Neuroradiology (J.F., T.I., M.P., U.G.), Medical Informatics (D.S., N.F., H.H.), and Neurosurgery (J.R.), University Medical Center Hamburg, Hamburg, Germany; and Department of Neuroradiology (J.V.B.), University of Oxford, John Radcliffe Hospital, Oxford, UK.

This work was supported by a research grant from BRACCO, Konstanz, Germany and by the Deutsche Forschungsgemeinschaft (Fi 904/5-1). J.F. is grateful to the European Exchange Program of the European Society of Neuroradiology for supporting his stay at Oxford.

Please address correspondence to: Jens Fiehler, MD, PhD, Department of Neuroradiology, University Medical Center Hamburg-Eppendorf, Martinistr 52, 20246 Hamburg, Germany; e-mail: fiehler@uke.de

DOI 10.3174/ajnr.A1351

Table 1: Demographics

No.	Age	Sex	Nidal Volume (mL)	Feeding Artery			Spetzler Grade[20]	Cortical	Location	Side	Symptoms
				ACA	MCA	PCA					
1	55	M	40	−	+	+	4	Yes	Temporal	R	SAH >6 months ago
2	33	M	300	+	+	+	4	Yes	Parieto-occipital	L	Seizures + headache
3	42	M	330	−	+	+	5	Yes	Temporo-occipital	R	SAH >6 months ago
4	51	M	130	+	+	−	3	Yes	Frontal	L	Tinnitus left side pronounced
5	45	M	130	−	−	+	4	Yes	Occipital	L	Seizures + headache
6	28	M	50	+	+	+	5	Yes	Temporal	L	Seizures + stuttering
7	33	F	270	+	+	+	4	Yes	Frontoparietal	R	Seizures
8	22	F	20	−	+	+	3	Yes	Occipitotemporal	R	Seizures + visual field defects
9	22	M	70	−	+	−	3	No	Temporal	R	Seizures
10	17	F	100	+	−	−	3	No	Frontoparietal	L	Incidental
11	35	F	340	+	+	−	2	Yes	Parietal	L	Seizures + dysaesthesia
12	47	M	80	−	+	+	3	Yes	Temporal	L	Seizures
13	41	F	20	+	+	−	2	Yes	Parietal	L	Pulsatile headache
14	51	F	40	−	+	−	3	No	Basal ganglia	L	Aphasia
15	45	M	40	+	−	+	3	Yes	Frontoparietal	L+R	Intraventricular hemorrhage >6 months ago
16	52	M	10	−	−	+	2	Yes	Parapontine	R	SAH >6 months ago
17	31	F	30	−	+	−	3	Yes	Frontal	R	Seizures
18	40	M	10	−	+	+	4	Yes	Temporal	L	Seizures
19	22	M	120	−	+	+	1	Yes	Temporoparietal	L	Seizures
20	19	M	60	+	−	+	5	No	Corpus callosum	L	Incidental

Note:—SAH indicates subarachnoid hemorrhage; R, right, L, left; −, not involved; +, involved; ACA, anterior cerebral artery; MCA, middle cerebral artery; PCA, posterior cerebral artery.

Materials and Methods

Patients

Twenty consecutive patients with AVM (7 female, 13 male) with a median age of 37 years (range, 17–55 years) were enrolled in the study. Inclusion criteria were an AVM diagnosed by conventional digital subtraction angiography (DSA) and the absence of imaging evidence of parenchymal hemorrhage. Informed consent was obtained from all patients. We defined focal AVM effects to be present in patients presenting with either seizures and/or focal neurologic deficit (FND) (Table 1). The study was approved by the local institutional review board (No. 2706/2005).

Imaging

MR imaging measurements were performed on a 3T Trio (Siemens, Erlangen, Germany) scanner by using an 8-channel phased array head coil. Along with other sequences, we used the following:

1) 3D time-resolved echo-shared acquisition technique (TREAT; ie, 4D-MRA) was performed.[16] TREAT was performed by using a 3D fast low-angle shot sequence with TE/TR of 0.77/2.22 ms, in-plane image resolution of 2.8 × 1.9 mm, and section resolution of 5 mm. Parallel imaging with a generalized autocalibrating partially parallel acquisitions factor of 2 was applied. Contrast injection was performed by intravenous pump injection of 20-mL gadobenate dimeglumine (MultiHance; Bracco Atlanta Pharma, Konstanz, Germany) at 4 mL/s, followed by 20-mL isotonic saline. This technique allowed acquisition of one 3D dataset in 0.5 seconds.

2) 3D time-of-flight MRA (TOF-MRA) was performed with a magnetization transfer saturation pulse, a TR of 36 ms, a TE of 6 ms, a flip angle of 25°, 2 slabs with 32 partitions, an image in-plane image resolution of 0.47 × 0.47 mm, a section thickness of 0.5 mm, and a FOV of 150 × 200 mm.

3) Pulsed arterial spin-labeling (PASL) perfusion imaging was performed by using the technique described by Luh et al.[17] Arterial spins were labeled by a 10-cm inversion slab placed proximal to the imaged sections.

In addition, conventional DSA with 3 images per second in standard projections with injections in both internal carotid arteries (ICAs) and at least 1 vertebral artery was performed in all patients. The location of the AVM nidus was assigned by a neuroradiologist to ≥1 cerebral lobes and to the cortex, subcortex, or both on routine T2-weighted MR images.

Postprocessing

Segmentation of the Vessel System. Spatial resolution of the 4D MRA was comparatively low. For detailed segmentation of the vessel system and the quantification of the size and location of the AVM structure, the 3D TOF-MRA (Fig 1) with high spatial resolution and a superior blood-to-background contrast was used. The software system AnToNIa (Analysis Tool for Neuro Image Data), which allows both vessel structures and their hemodynamics to be visualized together was used for analysis of the AVM nidus and classification of vessels next to the nidus.

Perfusion in Vessel Territories. In the PASL images, the vascular territories of the anterior, middle, and posterior cerebral arteries (ACA, MCA, PCA) were delineated by a neuroradiologist (J.F.) in the affected and unaffected hemispheres after exclusion of the AVM nidus by using an established method.[18] Because the technique measures signal intensities in arbitrary values only, the ratio between hemispheres was calculated for each region of interest.

Perfusion around the Nidus. The AVM nidus was delineated manually by using the TOF-MRA source images (by T.I.), and 16 regions of interest of increasing 3D shells were mapped around the nidus. For this, the entire volume was then subdivided by 4 perpendicular planes (in the z-direction) so that a cross-section contained 8 "pieces-of-cake" (Fig 2), and the entire volume was subdivided into a symmetric upper and lower hemisphere, doubling the pieces of cake to 16. This complex shape was used for the definition of brain territories surrounding the nidus. We analyzed the course of the PASL signal intensity from the nidus to the periphery across the 16 concentric shells (separately for each of the 16 pieces of cake). The complex shape within the TOF-MRA was evaluated by 2 neuroradiologists in consensus (T.I. and J.F.), and sections that included ventricles or re-

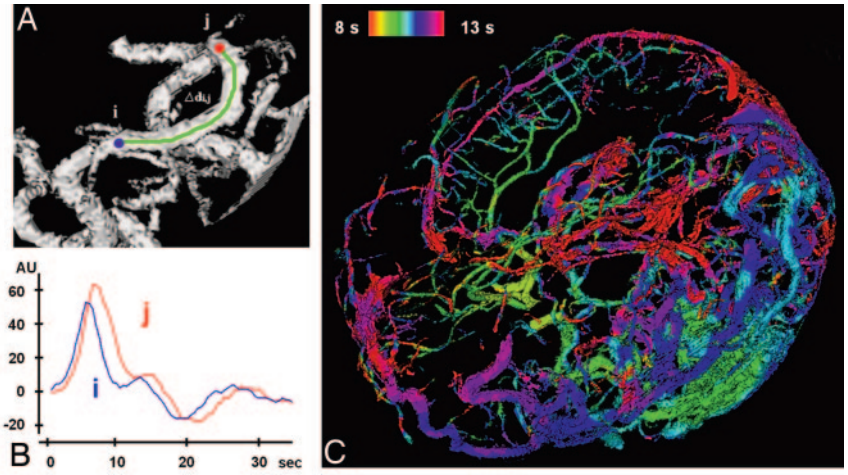

Fig 1. Temporal assignment of inflow time points. *A,* Section of an MIP of a vessel tree (based on 4D-MRA) with 2 manually selected locations (i and j). *B,* In maximum slope (in AUs) versus time (in seconds) curves, the time points for the maximum slope can be determined separately for i and j, and a delay can be calculated. *C,* The time points of those maxima are color-coded and projected onto the complete vessel tree of the AVM in the TOF-MRA.

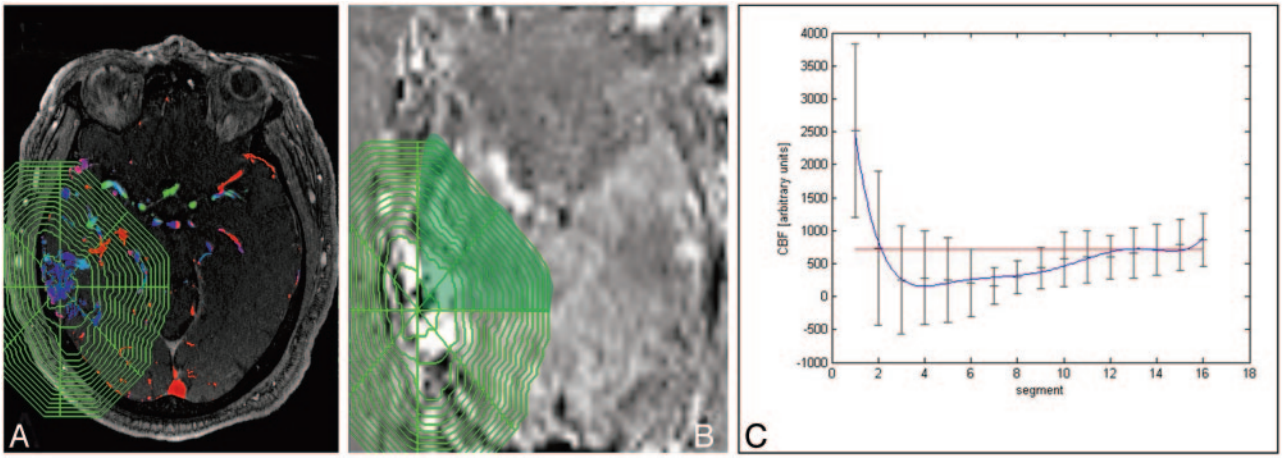

Fig 2. *A* and *B,* Determination of the PND after manual delineation of the AVM nidus in the TOF-MRA source images (*A*) and after the complex shape is transferred to the coregistered PASL map (*B*). *C,* Signal intensities for each piece of cake are determined in AUs in each segment beginning from the AVM nidus to the periphery. The segments outside the skull are excluded from further analysis. s indicates seconds.

gions outside the skull were excluded. After spatial coregistration, the complex shape was transferred to the PASL map. The signal intensities for each piece of cake were determined in arbitrary units (AU) in each segment, beginning from the AVM nidus to the periphery (Fig 2). The 4 points most remote from the nidus were used to fit a baseline to these points. A perinidal dip (PND) was defined as ≥20% reduction in signal intensity below the baseline, in sections immediately adjacent to the nidus.

For the additional visual inspection, the PASL maps were coregistered to the TOF-MRA source images and were searched for distinct cerebral blood flow (CBF) decreases in the perinidal or perivascular brain parenchyma of >5 mm in minimum diameter (Fig 3). The PASL maps were visually analyzed by 2 neuroradiologists in consensus (T.I. and J.F.) to find regions of clear perfusion impairment in the vicinity of a vascular structure of the AVM.

Quantification of Inflow. On the basis of the 4D-MRA, a hemodynamic reference curve was computed by calculating the normed mean curve of the temporal intensity curves of all vessel voxels on the basis of the manual segmentation of the vessel system. To determine a time point of inflow for a given voxel, we fitted the related temporal intensity curve of the signal intensity $s(t)$ to a reference curve $r(t)$, such that the sum of squared differences (SSD) $\Sigma_{i=1}[r(t) - f(s[r])[r]^2 = A + Bt$ was minimized, where A was the shift and B was the scaling factor. The curve-fitting algorithm was used to calculate the parameter of the linear transformation A and B such that $r(t) \sim f(s[r])$ depended on the SSD. A change in the scaling factor led to an offset, which was included in the calculation. The parameter B, which was estimated by this method, could then be used to define the inflow time point t_{tbi}. The entire method has been described in detail elsewhere.[19]

Combination of TREAT and TOF Image Information. A combination of information of hemodynamics based on the voxel-oriented analysis of the temporal intensity curve in TREAT 4D-MRA and anatomic vessel structures in high spatial resolution (3D TOF) requires the coregistration of both datasets. For this purpose, a 3D maximum intensity projection (MIP) with time (MIPt) was created on the basis of the 4D-MRA dataset (Fig 1). This projection leads to an advanced representation of the vessel system in the 3D MIPt (including helpful structures to improve the registration result). Thereafter, the resolution of the 3D MIPt was adapted to the 4D MRA by using a cubic resampling filter. Finally, the transformation field between the 2 datasets was calculated by using an affine 3D-3D registration method, with mutual information as a similarity measure. On the basis of the computed transformation field, all dynamic characteristics were transferred directly to the TOF-MRA image sequence and color-coded depending on the blood inflow characteristic (Fig 1*C*).

Inflow Time Measurements. For determination of inflow times within the macrovascular tree, a neuroradiologist (T.I.) placed a re-

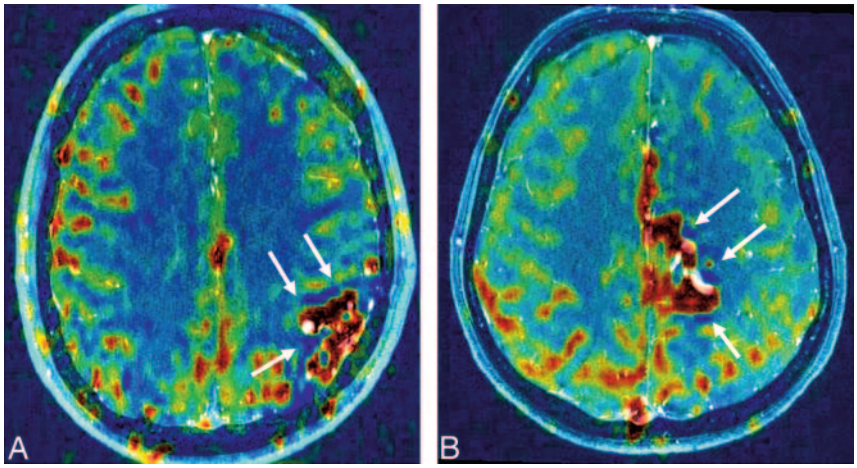

Fig 3. PASL maps (CBF-weighted) are coregistered to TOF-MRA source images. The patients either fulfill the 20% dip criterion (*A*, patient 18; 3647) or do not (*B*, patient 13; 3136). Nevertheless, dark-blue low CBF regions (*arrows*) are observed in both patients, suggesting local CBF decreases, possibly as a result of a local steal. Red indicates high CBF; dark blue, low CBF.

gion of interest on the major feeding artery and the major draining vein, both next to the AVM, and at standardized measuring points on the proximal ACA, MCA, PCA, and the transverse sinus (TS) of the affected and nonaffected sides. The transit time through the AVM was determined by the median time delay between the maximum slope in the feeding artery and vein. The absolute inflow time differences between the affected and nonaffected hemispheres were calculated for the ACA, MCA, and PCA, as well as ratios of the affected-versus-unaffected sides, to allow testing for correlation with the perfusion ratios derived from signal intensities in the PASL.

Statistics

Signal-intensity values of PASL images and inflow times in the 4D-MRA for the ACA, MCA, and PCA of the affected and nonaffected hemispheres were compared by the Mann-Wilcoxon *U* test. The relation of macrovascular inflow to microvascular perfusion was analyzed by correlating the vascular territories with their attributed feeding arteries by using the Spearman signed rank test. These CBF affected/CBF nonaffected ratios of the outlined vessel territories outside the AVM were then correlated with the affected/nonaffected ratios of inflow time points of the respective vessels (eg, $\text{Inflowtime}_{\text{ACAaffected/ACAnonaffected}}$ versus $\text{Perfusion}_{\text{ACAaffected/ACAnonaffected}}$). A univariate binary regression analysis was used to test the association of symptoms with AVM characteristics. Differences with P values $< .05$ were considered to be significant. Statistical calculations were performed by using the Statistical Package for the Social Sciences software, Verison 13.0 (SPSS, Chicago, Ill).

Results

DSA and Conventional Cross-Sectional Images

Cranial DSA images were available for all patients, and feeding arteries from the ICA or vertebrobasilar (VBA) circulations were included in the analysis. The AVMs were supplied by the ACA in 9 patients, the MCA in 15 patients, the PCA in 13 patients, and multiple territories in 14 patients. AVMs were categorized as those that were exclusively supplied by vessels of the ICA territory ($n = 7$), the VBA territory ($n = 2$), or a combination of ICA and VBA territories ($n = 11$). On the basis of anatomic T2-weighted MR imaging, the AVMs were subcortical in only 4 patients and cortical or both cortical and subcortical in 16 patients (Table 1).

Table 2: Perfusion ratios of affected-versus-nonaffected hemispheres for each vascular territory

Patient No.	ACA	MCA	PCA	PND (%)	Visible
1	1.01	0.95	1.02	–	Yes
2	1.02	0.98	0.99	–	Yes
3	1.02	0.94	0.88	–	Yes
4	–	1.00	1.09	–	Yes
5	0.93	0.96	0.90	–	Yes
6	0.98	0.93	1.00	–	Yes
7	0.96	0.95	0.90	–	No
8	1.03	1.00	0.89	–	Yes
9	0.99	0.94	0.94	–	Yes
10	0.96	0.95	0.90	49	Yes
11	1.00	1.01	0.89	–	Yes
12	1.19	0.98	0.94	39	No
13	0.96	0.97	0.93	–	Yes
14	0.95	0.98	0.97	52	Yes
15	0.99	0.99	0.99	–	No
16	1.09	1.02	1.02	–	Yes
17	1.01	1.00	0.99	–	Yes
18	0.99	0.98	1.02	62	Yes
19	0.97	0.93	1.01	–	Yes
20	0.98	0.92	0.82	78	Yes

Note:—PND indicates perinidal dip.

Perfusion in Vessel Territories

There was no difference in the perfusion ratio between of the affected and nonaffected hemispheres of the ACA territory (ratio, 1.00 ± 0.06; $P = .915$, Mann-Wilcoxon *U* test). In contrast, values were significantly decreased in the MCA (ratio, 0.96 ± 0.03; $P = .005$) and the PCA territories (ratio, 0.95 ± 0.07; $P = .001$). There was no difference in the ratios in the ACA, MCA, or PCA territories between patients with or without FND. One ACA territory measurement was not performed because of technical artifacts.

Perinidal Perfusion

In total, 167/320 segments fulfilled the quality criteria and were analyzed for perinidal perfusion. Five patients fulfilled the arbitrarily defined criterion for PND (ie, >20% decrease in baseline values around the nidus) (Table 2). The relative reduction in focal perfusion ranged from 37% to 78%. In these patients, AVMs were located at the subcortex in 3 (only 4

Table 3: Inflow times at predefined measuring points

	Affected Hemisphere (in seconds)	Contralateral Hemisphere (in seconds)	Ratio Affected/ Contralateral
ICA	10.8 ± 3.9	11.9 ± 4.2	0.96 ± 0.19
MCA	9.2 ± 2.5	9.5 ± 2.8	1.00 ± 0.33
ACA	10.2 ± 2.5	10.3 ± 2.7	0.94 ± 0.23
PCA	12.0 ± 5.0	12.4 ± 4.9	0.90 ± 0.16
TS	11.8 ± 3.0	11.6 ± 3.6	1.09 ± 0.94

Note:—ICA indicates internal carotid artery; TS, transverse sinus.

AVMs in the whole cohort were completely subcortical) (Table 1). There was no difference in the AVM circulatory time between patients with and without PND ($P = .807$, Mann-Wilcoxon U test). Additionally, visual inspection of the coregistered TOF and PASL maps found a clear perfusion impairment in the vicinity of a vascular structure of the AVM of high-flow arteries and veins in 17/20 patients (85%) (Fig 3).

Inflow Time Measurements

Absolute inflow times were 9.8 ± 2.8 seconds in the arterial feeder and 10.7 ± 3.2 seconds for the major draining vein. The mean difference between feeding artery and draining vein inflow times (ie, transit time) was 1.2 ± 1.1 seconds. The absolute mean hemispheric inflow time values are presented in Table 3. Differences in absolute values of inflow times between the hemispheres were significant for the PCA ($P < .001$, Mann-Wilcoxon U test), but not for the ACA and MCA ($P = .157$ and $P = .851$).

There was a significant negative correlation between AVM transit time and nidal volume ($R = -0.350$, $P = .021$). Inflow time ratios could not be calculated for patients when insufficient visibility precluded measurement in at least 1 of the paired vessels required for the hemispheric ratio (ACA, $n = 9$; MCA, $n = 7$; PCA, $n = 9$; TS, $n = 4$).

Correlation of Inflow Times and Perfusion in the Related Territories

There was a negative correlation between the affected/nonaffected perfusion and inflow time ratios in a combined analysis of all affected vascular territories ($R = -0.402$, $P = .015$, Fig 4). In a separate analysis of each vascular territory, only the PCA perfusion ratio was inversely correlated with the inflow time ratio (-0.662, $P = .026$).

Association of Clinical Symptoms with AVM Characteristics

In a univariate binary regression analysis, there was no statistically significant association of symptoms, presumed to be due to a focal AVM effect (composite seizures or focal neurologic deficit, $n = 12$, Table 1) with nidal volume, transit time, or PND.

Discussion

In summary, we observed a negative correlation between the contrast agent arrival times on a macrovascular level and the microvascular perfusion in the respective vascular territories (ie, the microvascular flow was decreased in the presence of a high flow in the vessels contributing to the AVM, Fig 4). We hypothesize that the macrovascular flow (and thus the inflow time) and degree of perfusion impairment in the AVM vascular territory are both determined by its arteriovenous pressure difference. The perfusion analysis of tissue immediately surrounding the AVM showed PND in 25% and a discernable but lesser flow decrease in a further 60% of patients (Table 2 and Fig 3). No correlation with clinical symptoms and the degree of perfusion impairment in the entire vascular territories or PND was observed, but for the latter, the numbers are too small to rule out such an association.

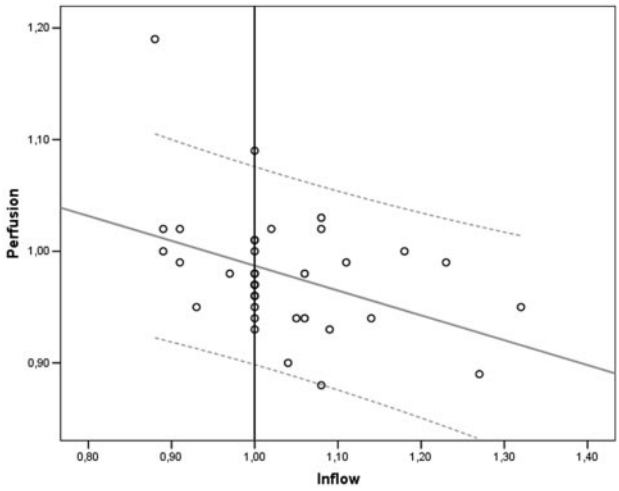

Fig 4. There is a negative correlation of the perfusion ratio with the inflow ratio in a combined analysis of all affected vascular territories ($R = -0.402$, $P = .015$). The gray line represents the regression line with 95% confidence intervals (dotted lines).

There is discordance among previous reports over whether perfusion abnormalities in the brain parenchyma of patients with AVM involve the territory of large arterial feeders or just the area in close proximity to the nidus.[7,13-15,21,22] Guo et al[13] reported a perinidal steal in brain AVMs and described 3 types of perfusion disturbance. In type 1, CBF and cerebral blood volume (CBV) ratios were increased in the immediate and remote perinidal regions. In type 2, CBF and CBV ratios were increased in the immediate and decreased in the remote perinidal regions; and in type 3, CBV and CBF ratios were decreased in both the immediate and remote perinidal regions. The authors used only the largest nidal section for measurement in a single section and did not correlate their findings with macrovascular flow. Previously, Prosenz et al[21] observed CBF decreases only in remote brain supplied by terminal branches of the pedicle artery, in contrast to Kader and Young,[22] who were unable to demonstrate altered CBF in angiographically discrete vascular territories and found no clear-cut territorial alteration in CBF ratios. In a recent study based on perfusion MR imaging, the mean transit time did not reveal any obvious hemodynamic disturbances in 18/20 patients.[14] This report contrasts with our finding of significant hemispheric CBF asymmetries. The absence of perifocal CBF abnormalities in previous studies may be due to shortcomings in previous imaging methods with lower spatial resolutions.[7,15]

It has been suggested that reduced arterial and raised venous pressures in AVM feeders are sufficient to compromise resting-state CBF adjacent to the AVM.[23] The inhomogeneous effect of the macrovascular AVM flow on the perfusion within the territory of the feeding artery in our study confirms such a second level of local perfusion impairment. We found the phe-

nomenon in most patients (85%). Such perinidal perfusion abnormalities have been ascribed to neuronal loss (and reduced metabolic demand) in chronically hypoperfused areas, rather than to hemodynamic steal effects.[7] The inhomogeneous distribution of discrete perfusion abnormalities can be better explained by local differences in the arteriolar angioarchitecture than by the hemispheric asymmetry and the arterioarterial redistribution on a macrovascular level that we observed. Both levels of perfusion impairment are visible in Fig 3. The local CBF decrease is compatible with recent histologic reports of a perinidal dilated capillary network in 85%–100% of patients with AVM[24,25] and may be due to an exhausted compensatory mechanism. These capillaries are connected not only to the nidus, feeding arteries, and draining veins via arterioles and venules but also to normal capillaries, arterioles, and venules. The perinidal brain parenchyma has been reported to show significant ischemic changes,[24,25] though a previous diffusion-weighted imaging study did not reveal perinidal ischemia in unselected patients with AVM.[14]

The conclusions that can be drawn from our study are limited by the low number of patients and high variability of brain AVMs. Variability in regional flow is likely to be related to multiple factors, including AVM size and flow rate, feeding artery pattern, availability of collaterals, venous pressure, metabolic demand, local anatomy, and others. AVM hemodynamics are difficult to quantify, particularly within or in close proximity to the nidus.[26] The regions of interest chosen in our study always contained mixtures of arteries, capillaries, veins, and intervening brain tissues and are subject to the effects of partial voluming. The temporal resolution of 0.5 seconds for the 4D MRA is suboptimal for the study of high-flow lesions such as AVMs. However, the postprocessing with the interpolation steps we used improves this temporal resolution.[20] Despite these caveats, the technique is based on TOF-MRA and 4D MRA sequences, which require <1 minute of imaging time. In the future, the method could be used to study the effects of treatment on macrovascular flow and perfusion and in pretreatment studies to assess the risk of postprocedure "breakthrough" hemorrhage. Moreover, the technique could also be useful for evaluating the effects of staged embolization on the extent and the magnitude of areas of perinidal flow impairment and to relate changes to clinical symptoms.

Conclusions

The significant perfusion impairment in vascular territories next to the AVM with an additional PND may reflect the existence of 2 levels of perfusion impairment in brain AVMs: a territorial and a microvascular perfusion disturbance. Although the gross hemispheric asymmetry in territorial perfusion appears to be caused by arterioarterial redistribution on a macrovascular level, the perivascular perfusion dip is inhomogeneously distributed within a single vascular territory and thus may result from low perfusion pressure in small arteries and arterioles because it correlates with levels of macrovascular flow through the AVM.

Acknowledgments

We gratefully acknowledge the support by the Hamburg MR imaging staff and technologists, especially from Ms Gyde Riepen. We thank H. Zeumer and M. Westphal for enduring and stimulating discussions.

References

1. Lasjaunias P, Manelfe C, Chiu M. **Angiographic architecture of intracranial vascular malformations and fistulas: pretherapeutic aspects.** *Neurosurg Rev* 1986;9:253–63
2. Norlén G. **Arteriovenous aneurysms of the brain: report of ten cases of total removal of the lesion.** *J Neurosurg* 1949;6:475–94
3. Taylor CL, Selman WR, Ratcheson RA. **Steal affecting the central nervous system**. *Neurosurgery* 2002;50:679–88, discussion 688–89
4. Symon L. **The concept of intracerebral steal.** *Int Anesthesiol Clin* 1969;7:597–615
5. Mast H, Mohr JP, Osipov A, et al. **"Steal" is an unestablished mechanism for the clinical presentation of cerebral arteriovenous malformations.** *Stroke* 1995;26:1215–20
6. Tyler JL, Leblanc R, Meyer E, et al. **Hemodynamic and metabolic effects of cerebral arteriovenous malformations studied by positron emission tomography.** *Stroke* 1989;20:890–98
7. Fink GR. **Effects of cerebral angiomas on perifocal and remote tissue: a multivariate positron emission tomography study.** *Stroke* 1992;23:1099–105
8. Guo WY, Pan DH, Liu RS, et al. **Early irradiation effects observed on magnetic resonance imaging and angiography, and positron emission tomography for arteriovenous malformations treated by gamma knife radiosurgery**. *Stereotact Funct Neurosurg* 1995;64(suppl 1):258–69
9. Kaminaga T, Hayashida K, Iwama T, et al. **Hemodynamic changes around cerebral arteriovenous malformation before and after embolization measured with PET.** *J Neuroradiol* 1999;26:236–41
10. Iwama T, Hayashida K, Takahashi JC, et al. **Cerebral hemodynamics and metabolism in patients with cerebral arteriovenous malformations: an evaluation using positron emission tomography scanning.** *J Neurosurg* 2002;97:1314–21
11. Takeuchi S, Kikuchi H, Karasawa J, et al. **Cerebral hemodynamics in arteriovenous malformations: evaluation by single-photon emission CT.** *AJNR Am J Neuroradiol* 1987;8:193–97
12. Takeuchi S, Abe H, Nishimaki K, et al. **Cerebral haemodynamic changes after endovascular treatment of arteriovenous malformations: evaluation by single-photon emission CT.** *Acta Neurochir (Wien)* 1994;127:142–50
13. Guo WY, Wu YT, Wu HM, et al. **Toward normal perfusion after radiosurgery: perfusion MR imaging with independent component analysis of brain arteriovenous malformations.** *AJNR Am J Neuroradiol* 2004;25:1636–44
14. Cronqvist M, Wirestam R, Ramgren B, et al. **Endovascular treatment of intracerebral arteriovenous malformations: procedural safety, complications, and results evaluated by MR imaging, including diffusion and perfusion imaging.** *AJNR Am J Neuroradiol* 2006;27:162–76
15. Herzig R, Bogousslavsky J, Maeder P, et al. **Intracranial arterial and arteriovenous malformations presenting with infarction: Lausanne Stroke Registry study.** *Eur J Neurol* 2005;12:93–102
16. Fink C, Ley S, Kroeker R, et al. **Time-resolved contrast-enhanced three-dimensional magnetic resonance angiography of the chest: combination of parallel imaging with view sharing (TREAT).** *Invest Radiol* 2005;40:40–48
17. Luh GY, Dean BL, Tomsick TA, et al. **The persistent fetal carotid-vertebrobasilar anastomoses.** *AJR Am J Roentgenol* 1999;172:1427–32
18. van der Zwan A, Hillen B, Tulleken CA, et al. **Variability of the territories of the major cerebral arteries.** *J Neurosurg* 1992;77:927–40
19. Forkert ND, Säring D, Illies T, et al. **Automatische Lokalisation und haemodynamische Charakterisierung von Gefaessstrukturen bei arteriovenoesen Malformationen.** In: Tolxdorff T, Braun J, Deserno, TM, et al, eds. *Bildverarbeitung für die Medizin 2008.* Berlin, Germany: Springer; 2008: 107–111
20. Spetzler RF, Martin NA. **A proposed grading system for arteriovenous malformations.** *J Neurosurg* 1986;65:476–83
21. Prosenz P, Heiss WD, Kvicala V, et al. **Contribution to the hemodynamics of arterial venous malformations.** *Stroke* 1971;2:279–89
22. Kader A, Young WL. **The effects of intracranial arteriovenous malformations on cerebral hemodynamics.** *Neurosurg Clin N Am* 1996;7:767–81
23. McMahon JH, Morgan MK, Dexter MA. **The surgical management of contralateral anterior circulation intracranial aneurysms.** *J Clin Neurosci* 2001;8:319–24
24. Attia W, Tada T, Hongo K, et al. **Microvascular pathological features of immediate perinidal parenchyma in cerebral arteriovenous malformations: giant bed capillaries.** *J Neurosurg* 2003;98:823–27
25. Sato S, Kodama N, Sasaki T, et al. **Perinidal dilated capillary networks in cerebral arteriovenous malformations**. *Neurosurgery* 2004;54:163–68, discussion 168–70
26. Hademenos G, Massoud T, Vinuela F. **A biomathematical model of intracranial arteriovenous malformations based on electrical network analysis: theory and hemodynamics.** *Neurosurgery* 1996;38:1005–15